Windy Mars: A dynamic planet as seen by the HiRISE camera

N. T. Bridges,[1] P. E. Geissler,[2] A. S. McEwen,[3] B. J. Thomson,[1] F. C. Chuang,[4] K. E. Herkenhoff,[2] L. P. Keszthelyi,[2] and S. Martínez-Alonso[5]

[1]   With a dynamic atmosphere and a large supply of particulate material, the surface of Mars is heavily influenced by wind-driven, or aeolian, processes. The High Resolution Imaging Science Experiment (HiRISE) camera on the Mars Reconnaissance Orbiter (MRO) provides a new view of Martian geology, with the ability to see decimeter-size features. Current sand movement, and evidence for recent bedform development, is observed. Dunes and ripples generally exhibit complex surfaces down to the limits of resolution. Yardangs have diverse textures, with some being massive at HiRISE scale, others having horizontal and cross-cutting layers of variable character, and some exhibiting blocky and polygonal morphologies. ''Reticulate'' (fine polygonal texture) bedforms are ubiquitous in the thick mantle at the highest elevations. **Citation:** Bridges, N. T., P. E. Geissler, A. S. McEwen, B. J. Thomson, F. C. Chuang, K. E. Herkenhoff, L. P. Keszthelyi, and S. Martínez-Alonso (2007), Windy Mars: A dynamic planet as seen by the HiRISE camera, *Geophys. Res. Lett.*, *34*, L23205, doi:10.1029/2007GL031445.

1.   Introduction

[2]   HiRISE, with a resolution of $\sim$30 cm/pixel, large swath width of $\sim$6 km, high signal-to-noise (typically >100:1), and other advanced capabilities, is the most sensitive camera ever put into orbit around another planet [*McEwen et al.*, 2007]. It is ideal for studying small features, such as those associated with aeolian processes. This paper reports on significant HiRISE observations of Martian aeolian landforms within the first six months of MRO's Primary Science Phase.

2.   Dune and Ripple Textures

[3]   HiRISE reveals previously unseen complex surface textures on dunes and ripples. Dunes are saltation deposits, with the coarsest grains in the troughs, whereas ripples are formed from saltation-induced creep, with the coarsest grains at the crests. Ripples are always oriented transverse to the wind, whereas the shape of dunes is more complex and is dependent upon particle supply and wind regime [*Bagnold*, 1941]. Here we use the term "bedform" when one form cannot be confidently distinguished from another. Up to 3 orders of superposed bedforms are commonly seen in HiRISE images (Figure 1). The first order (T_1) is the trend marked by the large dune or ripple crests. Higher orders, commonly at sub-orthogonal orientations, are referred to as T_2 and T_3, following terrestrial nomenclature [*Warren and Kay*, 1987]. Similar patterns are seen on Earth dunes [*Warren and Kay*, 1987; *Bristow et al.*, 2000], with T_2 and T_3 bedforms forming on time scales as short as a day. The higher order bedforms occur preferentially, but not exclusively, on the gentle slope, interpreted as the stoss (windward) face, of the lower order bedforms. These ordered features are present in most HiRISE images containing bedforms and are seen on transverse, barchan, and dome dunes and as well as on many ripples. In lower resolution Mars Orbiter Camera (MOC) images, only bedforms down to T_2 order could be resolved and, at the limit of resolution, were sometimes misinterpreted as features with a different origin. For example, in Herschel Crater ($-14.7°$, $230.3°$W) the T_2 trend was interpreted as grooves formed by etching of an indurated T_1 dune surface [*Malin and Edgett*, 2001; *Schatz et al.*, 2006]. HiRISE shows that the T_2 trend does not correspond to erosional grooves, but rather to depositional bedforms, and reveals a population of T_3 bedforms perpendicular to T_2 (Figure 1b). The angle between the higher and lower order bedforms varies from orthogonal to nearly orthogonal. Where rock wind tails are visible, these point in the direction of the acute angle of the T_1-T_2 intersection, showing that sub-orthogonal higher order bedforms can be used as near-surface wind vanes (Figure 1d). The sub-orthogonal intersections are most likely caused by wind funneling within the topographic troughs between the T_1 bedforms, causing the T_2 bedforms that are farther downslope on the T_1 face to migrate at a greater rate than those upslope.

3.   Bedform Activity

[4]   Although the time-scale over which HiRISE has been observing Mars is thus far insufficient to measure bedform migration rates, insight is provided by comparing images to ground truth at the Mars Exploration Rover (MER) sites, as well as looking at fresh impact craters and gullies. Attempts at measuring bedform migration rates with MOC and previous imagers have been based on T_1 positions and have been unsuccessful, indicating that rates are generally less than about a meter per Mars year (however, recent observations from MOC over 5.5 years, although not measuring migration rates, do show disappearance of two dome dunes and shrinkage of another [*Bourke and Edgett*, 2006; *Bourke et al.*, 2007]). Comparison of HiRISE and *Spirit* Pancam images in the Columbia Hills in Gusev Crater shows that T_2 ripples are oriented in the same direction as ventifact

[1]Jet Propulsion Laboratory, California Institute of Technology, Pasadena, California, USA.
[2]U.S. Geological Survey, Flagstaff, Arizona, USA.
[3]Lunar and Planetary Laboratory, University of Arizona, Tucson, Arizona, USA.
[4]Planetary Science Institute, Tucson, Arizona, USA.
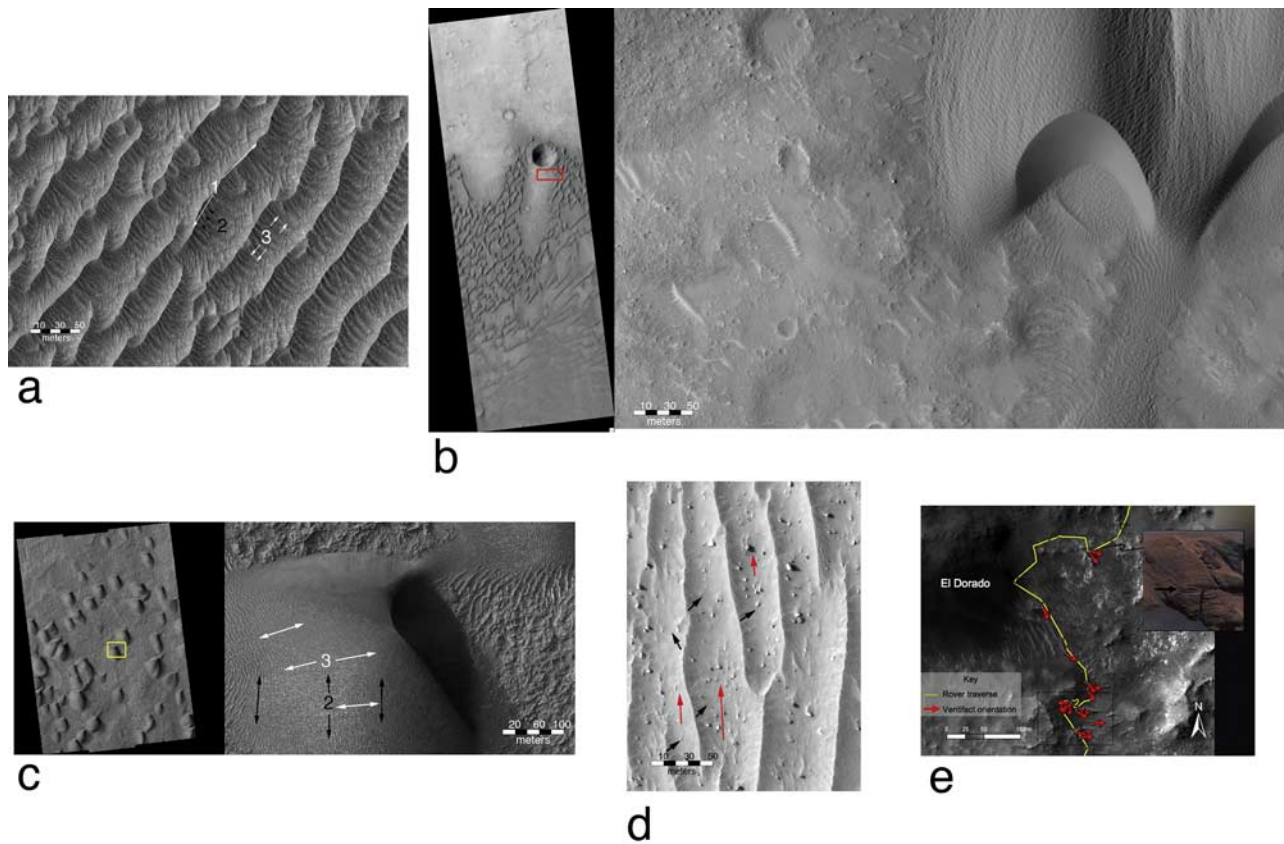[5]Department of Geological Sciences, University of Colorado, Boulder, Colorado, USA.

Figure 1. Bedform textures seen by the HiRISE camera. Here and in other figures the latitudes and longitudes refer to the center of the HiRISE footprint and north is at top. (a) Bedforms in Melas Chasma. Numbers refer to order of bedforms (1 = lowest order), with the arrows parallel to their crests (HiRISE image PSP_001443_1695; 10.4°S, 74.3°W). (b) Barchanoid dunes within Herschel Crater. (left) The complete HiRISE image. (right) A close-up of the red box, showing superposed bedforms on a dune and the adjacent sand sheet; these bedforms had been previously identified in MOC data as erosional grooves (PSP_002728_1645; 15.1°S, 228.1°W) (c) Tear-drop-shaped domical dunes in Wirtz Crater showing superposed T_2 (black arrows) and T_3 (white arrows) bedforms (PSP_001415_1315; 45.0°S, 25.3°W). (d) Ripples of order T_1 and T_2 within a crater inside Proctor Crater. Red arrows show orientation of rock wind tails. Black arrows show orientation of crests of T_2 ripples, which make a sub-orthogonal intersection with the larger T_1 ripples (PSP_003101_1320; 47.8°S, 329.3°W). (e) Ripples in the Columbia Hills with *Spirit* traverse shown in yellow and ventifact orientations shown by red arrows. Inset shows a Pancam image of ventifact flute on a rock (Sol 697). Note the alignment between ventifact features and 2nd order ripple trends (PSP_002133_1650; 14.6°S, 184.5°W).

abrasion features [*Thomson and Bridges*, 2007] (Figure 1e). Based on the superposition of the T_2 ripples on the T_1 ripples, this indicates that T_2, the ventifacts, and the wind regime that formed them are more recent than T_1. Coarse granules emplaced at the crests of T_1 ripples from saltation-induced creep tend to anchor the bedforms [*Sullivan et al.*, 2007], possibly followed by increases in cohesion, resulting in very slow subsequent migration. Particles on the stoss and lee side of the ripples are dominated by sand, which can potentially be saltated if friction speeds are great enough. Near-surface winds will be funneled by the 1st order ripple topography, constraining sand movement to the orthogonal direction, forming T_2 bedforms. Channeling of near-surface winds by ripples has also been proposed at the Opportunity site [*Sullivan et al.*, 2007]. It is unclear if dunes and T_2 ripples are active in all, or even most, cases. For example, prominent T_2 ripples are seen in many polar dunes, which some authors consider anchored by ice [*Bourke*, 2005; *Feldman et al.*, 2007].

[5] Bedforms are younger than the surfaces they superpose. The presence or absence of bedforms on demonstrably young features therefore provides insight into the rates of aeolian modification. Twenty very young (4 to 6 years old) craters on Mars have been previously reported [*Malin et al.*, 2006] and several more have been found at the time of this writing. HiRISE images show that all but one of these craters lack obvious aeolian bedforms, although some are too small for discernment of fine details. Three have some aeolian modification in the form of wind streaks. The largest of the craters identified by *Malin et al.* [2006], however, has clear ripples, down to order T_2, in its interior (Figure S1a of the auxiliary material).[1] Although more recent analyses indicate that this particular crater may, in fact, be older than 4–6 years (M. Malin, personal communication, 2007), it nevertheless appears young, with a crisp rim and sur-

---
[1]Auxiliary materials are available in the HTML. doi:10.1029/2007GL031445.

rounded by a field of angular boulders that are interpreted as relatively unaltered ejecta blocks. Several other possibly very young craters that are less than a kilometer in diameter and have a fresh morphology, similar to that shown in Figure S1a, have been imaged by HiRISE. These have bedforms in their interior (Figure S1b). Taken together, these observations demonstrate that aeolian activity in the crater interior occurs at a faster rate than crater rim and ejecta block modification. Studies at the MER landing sites indicate a two-stage crater gradation process, with the first marked by aeolian stripping of fine grained ejecta and deposition of the fines in the crater interior [*Grant et al.*, 2006]. The second stage is characterized by the trapping of regional sand from bedforms migrating on the surface into craters and other topographic lows and occurs over a much longer time scale [*Golombek et al.*, 2006]. This model is supported by HiRISE images down to small scales, where the presence of bedforms in fresh craters is independent of the abundance of bedforms outside of the crater (Figures S1a and S1b), with older craters serving as sand traps (Figure 1b).

[6] Ripples are also seen abutting the walls and intruding into some gully channels in Russell Crater (Figure S1c). The gullies appear fairly fresh, and are therefore presumably young. Where ripples are seen within the channels, the channel walls are more degraded compared to other channels without ripples. This indicates that the channels are being modified by the wind on a time scale comparable to the formation of new gullies.

4. Insight Into the Origin and Modification of Etched Materials

[7] Yardangs, elongated wind eroded landforms, have been known on Mars since Mariner 9 [*McCauley*, 1973]. Their largest concentration is within the Medusae Fossae Formation (MFF), an equatorial stratigraphic unit of Amazonian age [*Scott and Tanaka*, 1982]. The origin and composition of the MFF, and similar materials clearly eroded into yardangs. is not known, but candidates include indurated volcanic ash [*Ward*, 1979; *Scott and Tanaka*, 1982; *Wells and Zimbelman*, 1997; *Bradley et al.*, 2002; *Hynek et al.*, 2003] or dehydrated lags of former dust-ice mixtures [*Schultz and Lutz*, 1988]. Aeolian processes are judged as dominant in forming and modifying the materials, with airfall being the primary depositional mechanism in most models, later followed by material removal by deflation and abrasion. Curvilinear ridges identified in Aeolis Mensae [*Edgett and Williams*, 2004; *Williams and Edgett*, 2005] and the western MFF [*Burr et al.*, 2006] may be inverted channels, indicating that fluvial processes may have also modified these deposits.

[8] From HiRISE images, scalloped and fluted morphologies are evident in many etched materials and, in analogy to yardangs on Earth, are indicative of wind erosion (Figure 2a). These textures, noted in earlier MOC observations, can be more clearly described with HiRISE. In addition, we report new results that include finer textures that give insight into the origin (as opposed to the removal mechanism) of etched materials and outcrop distribution and size at high resolution. For example, many outcrops appear fairly massive, even at HiRISE scale (down to 25–32 cm/pixel; Figure 2a). Dark slope streaks, interpreted as

resulting from the removal of dust from a darker substrate [*Sullivan et al.*, 2001], are more common in massive exposures and suggest that dust deposits here are thick enough to cover textures seen in other etched materials. Horizontal bedding is clearly visible in other outcrops. Although some layering in MFF materials was apparent in lower resolution MOC images [*Sakimoto et al.*, 1999; *Bradley et al.*, 2002], in HiRISE bedding is resolved at scales of meters to decimeters, commonly expressed in outcrop as topographic benches (Figure 2b and Figure S2). This differential erosion suggests that material strength varies with stratigraphic position, indicating different primary material properties, mode of deposition, or exposure age. In other examples, the materials are blocky, exposed as either distinct horizontal or cross-cutting layers (Figure 2b), or comprising entire outcrops (Figure 2c). Finally, sub-decameter-scale polygonal textures are observed, such as on "White Rock" within Pollack Crater (Figure 2d). Many of the polygons appear raised.

[9] We propose that both the massive and bedded textures are consistent with an airfall origin of particulate material, in analogy to airfall tuffs on Earth that have similar morphologies. Whether the massive outcrops represent a true texture is not known, as the presence of slope streaks suggests that dust covers bedding and other textures. A dust or duricrust cover is consistent with thermal inertia and albedo measurements of the MFF [*Mellon et al.*, 2000; *Putzig et al.*, 2005]. The bedding may be caused by variable primary compositions, grain sizes, or exposure ages, which should influence the degree of cementation, leading to duricrust formation during the time the beds were at the surface. We propose that the blocky layers are either rock or strongly cemented material. A rocky origin for the layers could represent an unconformity during which the more massive airfall material ceased deposition and rocky material was laid down, with volcanic, fluvial, and impact origins all possible. The cross-cutting layers could be dikes or faults indurated by fluids, in either case indicating material of sufficient strength to propagate stresses. The polygonal forms bear some resemblance to star dunes seen within craters and reticulate bedforms in the summit calderas in Tharsis and Elysium (see next section and Figure 3). Star dunes form from the action of winds from several directions [*McKee*, 1979], which is common within trapped depressions like craters and calderas where wind flow can be reversed by topography [*Rafkin et al.*, 2001]. These bedforms, trapped within topographic lows, may be more easily lithified than dunes and ripples on the plains. Therefore, the polygonal morphology seen on some yardang/mantle material could represent cemented aeolian bedforms that have subsequently been partially abraded and deflated. This is consistent with TES results that indicate that White Rock, which is located within a crater, is a weakly cemented aeolian sediment [*Ruff et al.*, 2001].

[10] HiRISE reveals etched materials down to the limit of resolution (Figure S2a). With MFF outcrop areas as large as $\sim 10^4$ km^2, this indicates a range over at least 8 orders of magnitude in scale. Some of the small outcrops have circular perimeters, with a smaller fraction having raised rims (Figure S2a). Their morphology mirrors that seen filling larger craters, such as the one in the Figure S2 overview image. This suggests that impact craters within
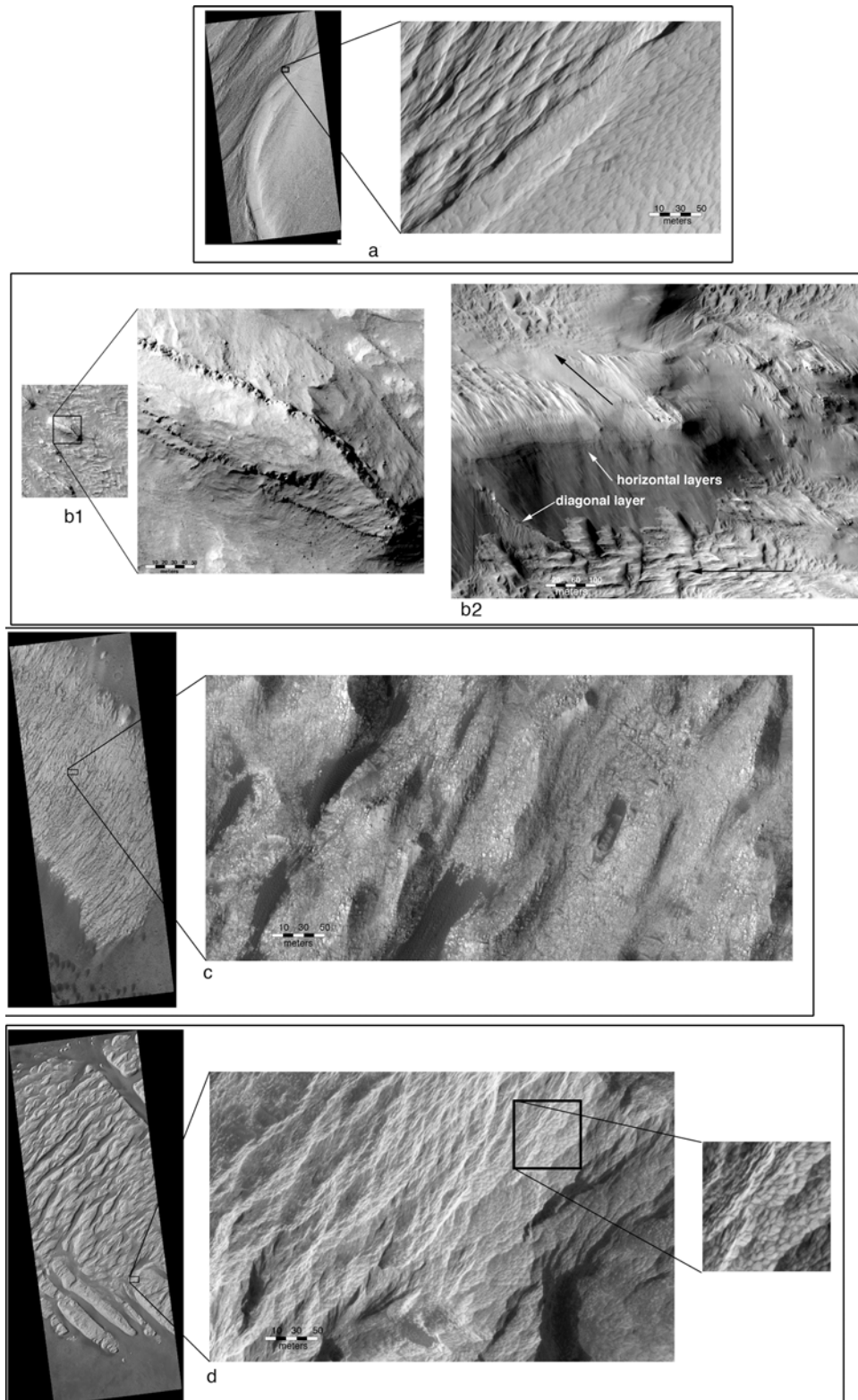
Figure 2. Yardangs showing a suite of textures. (a) MFF etched material within Nicholson Crater in Lucus Planum (PSP_002752_1800; 0.03°N; 164.8°W). (b) Yardangs exhibiting prominent horizontal and diagonal bedding (b1: TRA_000828_1805; 0.5°N, 217.9°W; Elysium Planitia; b2: TRA_000865_1905; 10.1°N, 148.5°W; outliers of Gordii Dorsum). Black arrows in b2 show directions of inferred winds believed to have formed the yardang texture. (c) Yardang interior deposit with a blocky texture in Trouvelot Crater in Arabia Terra (PSP_003287_1955; 5.4°N, 13.2°W). (d) "White Rock" in Pollack Crater in Terra Sabaea (PSP_002099_1720; 8.0°S, 335.0°W). (left) The entire HiRISE images, with the box indicating the location of the enlargements shown in the central and right panels; the latter shows an example of polygonal texture in detail.
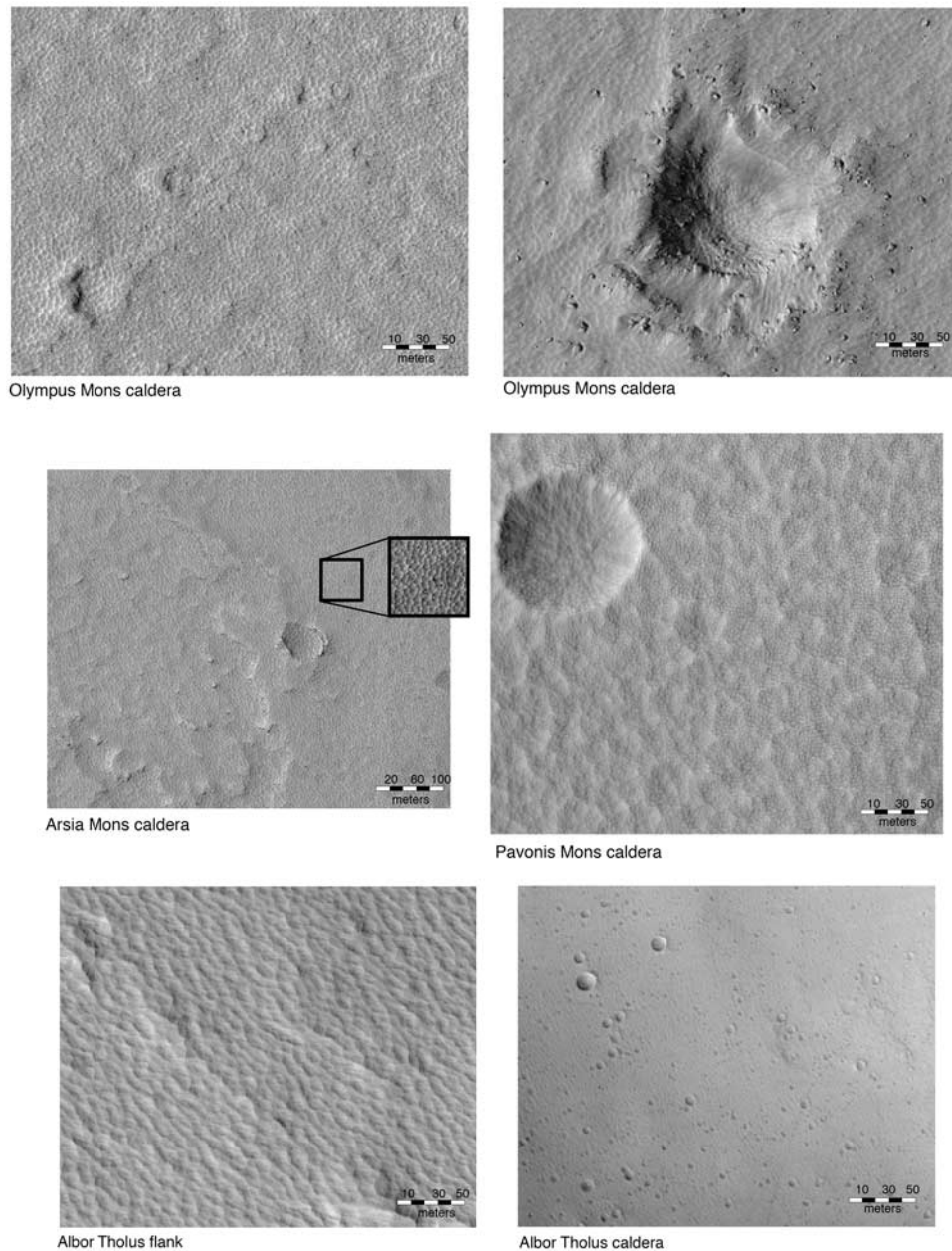
Figure 3. Bedforms of the "reticulate" morphology on high elevation volcanoes. The Arsia Mons image box shows the outline of a 2x enlargement, stretched sub-frame at right. Only the Arbor Tholus caldera lacks bedforms. (Arsia: PSP_002157_1715; Pavonis: PSP_002249_1805; Olympus: PSP_001920_1990; Albor Tholus: PSP_003492_1995).

and mantled by etched material are protected from deflation by a hardened crater rim, such that the circular interior is preserved after the surrounding terrain is stripped. An analogous stripping processes may explain the similar morphology of Home Plate (interpreted as volcanic structure or a filled impact crater) at the MER *Spirit* site [*Squyres et al.*, 2007].

5. High Elevation Bedforms

[11] MOC images showed that the high flanks and calderas of the Martian volcanoes are heavily mantled [*Malin and Edgett*, 2001]. The elevations of these edifices range from ~10 to 21 km, corresponding to atmospheric pressures of about 2 to less than 1 mb (1/1000th Earth atmospheric pressure). The observed mantle is consistent with earlier Viking infrared thermal mapper data showing that the summit regions have some of the lowest thermal inertia values on the planet, indicating fine (~2–40 μm) dust [*Christensen*, 1986]. However, the thermal inertial values do not have a unique interpretation, so it is possible that dust/rock mixtures or duricrust could also exist [*Bridges*, 1994]. The large seasonal variability and diurnal differences in the apparent thermal inertia on the volcanoes indicates a heterogeneous surface [*Putzig and Mellon*, 2007]. Most HiRISE images of the calderas and flanks of the Tharsis and Elysium Montes show a surface covered in bedforms with an integrated polygonal, or "reticulate,"

structure (Figure 3). One notable exception is the caldera of Albor Tholus. If the reticulate surfaces formed from saltation processes, it would be surprising given our understanding of aeolian physics in low density atmospheres. Threshold curves show that the friction speed needed to saltate particles increases as particle size (for $\sim$<100 μm) decreases and as atmospheric pressure decreases [*Greeley et al.*, 1976; *Iversen and White*, 1982]. The high elevation volcanoes are not where current surface shear stresses predicted by GCMs should induce saltation or dust lifting [*Haberle et al.*, 2003]. Saltation of sand-size material even under more favorable conditions (e.g., standard Martian pressures of $\sim$6 mb and the fastest wind speeds measured by the Viking and Pathfinder landers) is difficult. With pressures lower by up to an order of magnitude at the high elevations of the volcano summits and particle sizes less than fine sand, this is even more problematic. One possibility is that bedforms formed under a different Martian climate in the past, when atmospheric density was greater. Alternatively, the features may have been produced under present conditions. A surface having some cobbles (below HiRISE resolution) to increase the surface shear stress, or aggregated sand-size duricrust that can more easily be saltated than dust [*Bridges*, 1994] is appealing, although even these scenarios are a challenge to our current understanding of aeolian physics under low pressure conditions.

6. Current Sand Movement at Victoria Crater

[12] HiRISE has proven critical to understanding the present day aeolian activity at Victoria Crater in Meridiani Planum, the site of surface investigations by the MER rover *Opportunity*. Prominent wind streaks issue from embayments at the north end of the crater (Figure S3). The serrated rim may have formed by abrasion from windblown sand. Comparison of HiRISE with earlier MOC images show slight changes in the orientation and relative brightness of the streaks, indicating current activity. The streaks trend in the direction of northern summer winds and a fundamental question had been whether the streaks were erosional (removal of bright dust from a darker substrate) or depositional (covering of dark sand on a brighter substrate). HiRISE images show dark bedforms inside the crater at the base of the alcove leading up to the streak (Figure S3). This suggests that the streaks are depositional, being composed of dark sand from the bedforms. The rate at which the streaks fade will give a quantitative measure of depositional and erosional activity. This will be monitored by HiRISE over the coming months and years.

References

Bagnold, R. A. (1941), *The Physics of Blown Sand and Desert Dunes*, 265 pp., Methuen, London.
Bourke, M. C. (2005), Alluvial fans on dunes in Kaiser Crater suggest niveo-aeolian and denivation processes on Mars, *Lunar Planet. Sci.*, XXXVI, 2373.
Bourke, M. C., and K. S. Edgett (2006), First evidence of dune movement on Mars, *Eos Trans. AGU*, *87*(52), Fall Meet. Suppl., Abstract P31B-0128.
Bourke, M. C., K. S. Edgett, and B. A. Cantor (2007), Recent aeolian dune changes on Mars, *Geomorphology*, in press.
Bradley, B. A., S. E. H. Sakimoto, H. Frey, and J. R. Zimbelman (2002), Medusae Fossae Formation: New perspectives from Mars Global Surveyor, *J. Geophys. Res.*, *107*(E8), 5058, doi:10.1029/2001JE001537.
Bridges, N. T. (1994), Elevation-corrected thermal inertia and derived particle size on Mars and implications for the Tharsis Montes, *Geophys. Res. Lett.*, *21*, 785–788.
Bristow, C. S., S. D. Bailey, and N. Lancaster (2000), The sedimentary structure of linear sand dunes, *Nature*, *406*, 56–59.
Burr, D. M., R. M. E. Williams, J. Nussbaumer, and J. R. Zimbelman (2006), Multiple, distinct, (glacio?) fluvial paleochannels throughout the western Medusae Fossae Formation, Mars, *Lunar Planet. Sci.*, XXXVII, 1367.
Christensen, P. R. (1986), Regional dust deposits on Mars: Physical properties, age, and history, *J. Geophys. Res.*, *91*, 3533–3545.
Edgett, K. S., and R. M. E. Williams (2004), Valleys and channels in the Martian rock record, paper presented at Workshop on Mars Valley Networks, Smithsonian Inst., Kohala Coast, Hawaii, 11–14 Aug.
Feldman, W. C., M. C. Bourke, R. C. Elphic, S. Maurice, T. H. Prettyman, D. J. Lawrence, and J. J. Haggerty (2007), Constraints on the structure and composition of sand dunes within Olympia Undae using Mars Odyssey Neutron Spectrometer data, *Lunar Planet. Sci.*, XXXVIII, 2311.
Golombek, M. P (2006), Geology of the Gusev cratered plains from the Spirit rover transverse, *J. Geophys. Res.*, *111*, E02S07, doi:10.1029/2005JE002503.
Grant, J. A., et al. (2006), Crater gradation in Gusev crater and Meridiani Planum, Mars, *J. Geophys. Res.*, *111*, E02S08, doi:10.1029/2005JE002465.
Greeley, R., B. White, R. Leach, J. Iversen, and J. Pollack (1976), Mars: Wind friction speeds for particle movement, *Geophys. Res. Lett.*, *3*, 417–420.
Haberle, R. M., J. R. Murphy, and J. Schaeffer (2003), Orbital change experiments with a Mars general circulation model, *Icarus*, *161*, 66–89.
Hynek, B. M., R. J. Phillips, and R. E. Arvidson (2003), Explosive volcanism in the Tharsis region: Global evidence in the Martian geologic record, *J. Geophys. Res.*, *108*(E9), 5111, doi:10.1029/2003JE002062.
Iversen, J. D., and B. R. White (1982), Saltation threshold on Earth, Mars, and Venus, *Sedimentology*, *29*, 111–119.
Malin, M. C., and K. S. Edgett (2001), Mars Global Surveyor Mars Orbiter Camera: Interplanetary cruise through primary mission, *J. Geophys. Res.*, *106*, 23,429–23,570.
Malin, M. C., K. S. Edgett, L. V. Posiolova, S. M. McColley, and E. Z. N. Dobrea (2006), Present-day impact cratering rate and contemporary gully activity on Mars, *Science*, *314*, 1573–1577.
McCauley, J. F. (1973), Mariner 9 evidence for wind erosion in the equatorial and mid latitude regions of Mars, *J. Geophys. Res.*, *78*, 717–751.
McEwen, A. S., et al. (2007), Mars Reconnaissance Orbiter's High Resolution Imaging Science Experiment (HiRISE), *J. Geophys. Res.*, *112*, E05S02, doi:10.1029/2005JE002605.
McKee, E. D. (1979), Introduction to a study of global sand seas, in *A Study of Global Sand Seas*, edited by E. D. McKee, *U.S. Geol. Surv. Prof. Pap.*, *1052*, 3–17.
Mellon, M. T., B. M. Jakosky, H. H. Kieffer, and P. R. Christensen (2000), High-resolution thermal inertia mapping from the Mars Global Surveyor Thermal Emission Spectrometer, *Icarus*, *148*, 437–455.
Putzig, N. E., and M. T. Mellon (2007), Apparent thermal inertia and the surface heterogeneity of Mars, *Icarus*, *191*, 68–94, doi:10.1016/j.icarus.2007.05.013.
Putzig, N. E., M. T. Mellon, K. A. Kretke, and R. E. Arvidson (2005), Global thermal inertia and surface properties of Mars from the MGS mapping mission, *Icarus*, *173*, 325–341.
Rafkin, S. C. R., R. M. Haberle, and T. I. Michales (2001), The Mars regional atmospheric modeling system: Model description and selected simulations, *Icarus*, *151*, 228–256.
Ruff, S. W., P. R. Christensen, R. N. Clark, H. H. Kieffer, M. C. Malin, J. L. Bandfield, B. M. Jakosky, M. D. Lane, M. T. Mellon, and M. A. Presley (2001), Mars' "White Rock" feature lacks evidence of an aqueous origin: Results from Mars Global Surveyor, *J. Geophys. Res.*, *106*(E10), 23,921–23,928.
Sakimoto, S. E. H., H. V. Frey, J. B. Garvin, and J. H. Roark (1999), Topography, roughness, layering, and slope properties of the Medusae Fossae Formation from Mars Orbiter Laser Altimeter (MOLA) and Mars Orbiter Camera (MOC) data, *J. Geophys. Res.*, *104*, 24,141–24,154.
Schatz, V., H. Tsoar, K. S. Edgett, E. J. R. Parteli, and H. J. Herrmann (2006), Evidence for indurated sand dunes in the Martian north polar region, *J. Geophys. Res.*, *111*, E04006, doi:10.1029/2005JE002514.

Schultz, P. H., and A. B. Lutz (1988), Polar wandering on Mars, *Icarus*, *73*, 91–141.

Scott, D. H., and K. L. Tanaka (1982), Ignimbrites of Amazonis Planitia region of Mars, *J. Geophys. Res.*, *87*, 1179–1190.

Squyres, S. W., et al. (2007), Pyroclastic activity at Home Plate in Gusev Crater, Mars, *Science*, *316*, 738–742.

Sullivan, R., P. Thomas, J. Veverka, M. Malin, and K. S. Edgett (2001), Mass movement slope streaks imaged by the Mars Orbiter Camera, *J. Geophys. Res.*, *106*, 23,607–23,633.

Sullivan, R., R. Arvidson, J. Grotzinger, A. Knoll, M. Golombek, B. Joliff, S. Squyres, and C. Weitz (2007), Aeolian geomorphology with MER Opportunity at Meridiani Planum, Mars, *Lunar Planet. Sci.*, *XXXVIII*, 2048.

Thomson, B. J., and N. T. Bridges (2007), Rock abrasion features in the Columbia Hills, *Lunar Planet. Sci.*, *XXXVIII*, 1780.

Ward, A. W. (1979), Yardangs on Mars: Evidence of recent wind erosion, *J. Geophys. Res.*, *84*, 8147–8166.

Warren, A., and S. Kay (1987), Dune networks, *Spec. Publ. Geol. Soc. London*, *35*, 205–212.

Wells, G. L., and J. R. Zimbelman (1997), Extraterrestrial arid surface processes, in *Arid Zone Geomorphology: Process, Form and Change in Drylands*, 2nd ed., edited by D. S. G. Thomas, pp. 659–690, John Wiley, New York.

Williams, R. M. E., and K. S. Edgett (2005), Valleys in the Martian rock record, *Lunar Planet. Sci.*, *XXXVI*, 1099.

N. T. Bridges and B. J. Thomson, Jet Propulsion Laboratory, California Institute of Technology, Mail Stop 183-501, 4800 Oak Grove Drive, Pasadena, CA 91109, USA. (nathan.bridges@jpl.nasa.gov)

F. C. Chuang, Planetary Science Institute, 1700 E. Fort Lowell Road, Suite 106, Tucson, AZ 86719, USA.

P. E. Geissler, K. E. Herkenhoff, and L. P. Keszthelyi, U.S. Geological Survey, 2255 N. Gemini Drive, Flagstaff, AZ 86001, USA.

S. Martínez-Alonso, Department of Geological Sciences, University of Colorado, C.B. 392, Boulder, CO 80309-0392, USA.

A. S. McEwen, Lunar and Planetary Laboratory, University of Arizona, Tucson, AZ 85711, USA.